Q-space analysis of scattering by particles: a review

Christopher M. Sorensen

Q-Space Analysis of Scattering by Particles: A Review

Christopher M. Sorensen
Department of Physics
Kansas State University
Manhattan KS 66506 USA
sor@phys.ksu.edu

Abstract. This review describes and demonstrates the Q-space analysis of light scattering by particles. This analysis involves plotting the scattered intensity versus the scattering wave vector $q = (4\pi/\lambda) \sin(\theta/2)$ on a double log plot. The analysis uncovers power law descriptions of the scattering with length scale dependent crossovers between the power laws. It also systematically describes the magnitude of the scattering and the interference ripple structure that often underlies the power laws. It applies to scattering from dielectric spheres of arbitrary size and refractive index (Mie scattering), fractal aggregates and irregularly shaped particles such as dusts. The benefits of Q-space analysis are that it provides a simple and comprehensive description of scattering in terms of power laws with quantifiable exponents; it can be used to differentiate scattering by particles of different shapes, and it yields a physical understanding of scattering based on diffraction.

1. Introduction

The scattering of light from particles is an important method for *in situ*, non-invasive, real time characterization of the scattering particles. Particle size, morphology, refractive index and concentration can be determined under the ideal situation in which the scattering magnitude and angular distribution are fully characterized and the inverse problem of using such data to determine these properties can be solved. However, whereas the task of calculating the scattering patterns from particles of known size, shape and refractive index has seen impressive advances, the inverse problem of going from the scattering back to the particle remains formidable.

Another very important application for light scattering is to understand the effects of particulate scattering and absorption in the Earth's atmosphere on the global environment. For this application the impressive advances for calculating scattering from a wide variety of particles mentioned above can be very useful. However, increasing particle complexity requires increasingly complex calculations which hamper their facile application to the point where approximations are often applied. Moreover, these complex solutions yield little or no physical insight into the scattering process.

Thus it seems that the field of light scattering could use a new perspective that could quantitatively describe and differentiate the scatterings from different types of particles. It could also use a description that would yield a physical picture of the scattering process, a desire spurred both by the practical need to predict simply scattering as new types of particles are encountered, and the more general motive to understand fundamentally this aspect of nature.

In this paper I review a method which provides a new perspective on light scattering. The method is a simple change in the manner by which to view the angular scattering patterns. Instead of plotting the scattered intensity versus the scattering angle, the new perspective plots the scattered intensity versus the magnitude of the scattering wave vector, and the plots are made log-log. This method is not all together new. It has a long history of application to small angle X-ray and neutron scattering, however, it was not applied to light scattering until we first applied it to Mie scattering from spheres more than a decade ago [1]. When we did, we discovered patterns in the scattering that involved power laws that had never been described before. More work followed both from our lab [2-6] and others [7-12]. Recent application to random nonspherical particle geometries [13-15] indicates that the usefulness of the new perspective might be wide spread. We call this new perspective "Q-space analysis".

2. The Scattering Wave Vector

As the name implies, the fundamental variable in the Q-space analysis is the scattering wave vector q. Thus it is very appropriate that our description of Q-space analysis starts with a description of the origin of q in scattering theory. We follow the description given in [16]. Consider a scalar wave incident upon a point-like scattering element, or scatterer, at $\vec{r}$ as drawn in Fig. 1. Since the scatterer is point-like, it scatters isotropically throughout space. The incident field at a position $\vec{r}$ is

$$E(\vec{r}) = E_0 \exp\left(i\vec{k}_i \cdot \vec{r}\right) \tag{1}$$

where i = √-1 and $\vec{k}_i$ is the incident wave vector, with magnitude $|\vec{k}_i| = 2\pi/\lambda$. The wave scatters in the direction of $\vec{k}_s$ toward the detector at R >> r. Then the field at the detector is a plane wave described by

$$E(\vec{R},\vec{r}) \sim E(\vec{r})\exp\left(i\vec{k}_s \cdot (\vec{R} - \vec{r})\right), \tag{2}$$

which with Eq. (1) yields

$$E(\vec{R},\vec{r}) \sim E_0 \exp\left(i\vec{k}_s \cdot \vec{R}\right)\exp\left(i(\vec{k}_i - \vec{k}_s) \cdot \vec{r}\right) \tag{3}$$
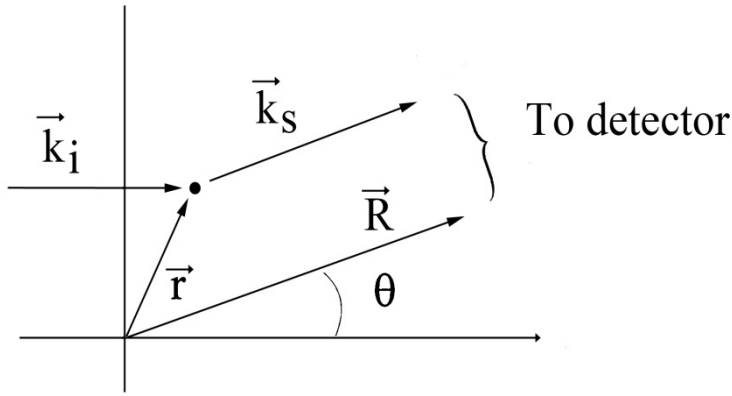

Figure 1. Diagram of light with an incident wave vector $\vec{k}_i$ scattering from a point scatterer at $\vec{r}$ into the scattering wave vector $\vec{k}_s$ at an angle θ directed to a distant detector.

We have dropped the equality for the proportionality because we don't know and don't need to know the strength of the scattering element at $\vec{r}$. The second term of Eq. (3) shows that the phase at the detector is a function of the position of the scattering element and the vector

$$\vec{q} = \vec{k}_i - \vec{k}_s \tag{4}$$

Equation (4) defines the *scattering wave vector* $\vec{q}$. Its direction is in the scattering plane from $\vec{k}_s$ to $\vec{k}_i$, and if the scattering is elastic, i.e. $|\vec{k}_i| = |\vec{k}_s|$, the magnitude of q is

$$q = 2k \sin(\theta/2) \tag{5a}$$

$$= (4\pi/\lambda) \sin(\theta/2) \tag{5b}$$

where θ is the scattering angle. Finally, we strip Eq.(3) to is essentials and write for the amplitude of the scattered wave

$$E_{sca}(\vec{q}, \vec{r}) \sim E_0 \exp(i\vec{q} \cdot \vec{r}) \tag{6}$$

The importance of $\vec{q}$ is that it describes how the phase at the detector depends on the position of the scatterer and the scattering angle. Any finite size object can be thought of as composed of a great many sub-volumes that act as point-like scatterers at various $\vec{r}$, a system of scatterers [16, 17]. Hence the total scattered wave is the sum of all the waves from the scatterers that make up the object. In taking this sum a baseline and very useful approximation can be made that the scattering from each individual scatterer of the object is so weak that it does not affect the other scatterers. Then each scatterer only sees the incident field and the interior of the scattering object is uniformly illuminated. This is the so-called Rayleigh-Gans or Rayleigh-Debye-Gans (RDG) [18- 21] approximation which leads to the total scattered field at the detector to be

$$E_{sca}(\vec{q}) \sim E_0 \sum \exp(i\vec{q}\cdot\vec{r}_i). \tag{7}$$

To convert the sum in Eq. (7) to an integral write the density function of the system of scatterers as

$$n(\vec{r}) = \sum \delta(\vec{r} - \vec{r}_i) \tag{8}$$

where $\delta(\vec{r})$ is the Dirac delta function. Then

$$\sum \exp(i\vec{q}\cdot\vec{r}) = \int \exp(i\vec{q}\cdot\vec{r})\, n(\vec{r})\, d\vec{r} \ . \tag{9}$$

Thus

$$E_{sca}(q) \sim E_0 \int \exp(i\vec{q}\cdot\vec{r})\, n(\vec{r})\, d\vec{r}. \tag{10}$$

In Eq. (10) we have anticipated the experimental situation where scattering will take place from an ensemble of particles of random orientations; thus the vector nature of q is eliminated. Equation (10) brings the realization that the functionality of the scattered wave under the RDG approximation is the Fourier transform of the real space structure of the scattering object. Given the reciprocity of the Fourier transform, it also implies that the Fourier transform of the wave scattered from the object is the real space structure functionality of the object. Indeed, the real space (r-space) and q-space (reciprocal space) descriptions of the object carry the same information only in different units.

One may also recognize that Eq. (10) describes diffraction from the scattering object, so it also brings the important realization that scattering under the RDG approximation is simply diffraction [22]. In this context it depends neither on the electromagnetic character of the light wave nor the electric properties of the scattering object as specified by its complex index of refraction.

The intensity of the scattered wave is the square of the complex scattering amplitude; hence the q-space functionality of the scattered intensity is the square of the Fourier transform of the real space structure. Intensity is what one usually detects in an experiment unless one "beats" the scattered wave against a "local oscillator", i.e. one does holographic detection of scattering [23].

To identify specifically the q-space functionality of the scattered intensity it is very useful to define a structure factor, S(q), as the Fourier transform of the real space structure of the object

normalized by the number of scatterers in the object, quantity squared. In integral notation the number of scatterers becomes the volume, V, of the object thus

$$S(q) = |V^{-1} \int \exp(i\vec{q} \cdot \vec{r}) \, n(\vec{r}) \, d\vec{r}|^2 \tag{11}$$

3. Scattering from Spheres.

3.1 The Rayleigh-Debye-Gans Limit.

The structure factor for a sphere of radius R can be calculated in spherical polar coordinates using Eq. (11) to find [18-21]

$$S(q) = [3(\sin u - u\cos u)/u^3)]^2 \tag{12}$$

where $u = qR$. This structure factor is directly proportional to the scattered intensity from a sphere of arbitrary radius and relative refractive index m when

$$\rho = 2kR|m - 1| < 1 \tag{13a}$$

and

$$|m - 1| \ll 1. \tag{13b}$$

Equation (13a) ensures that the phase across the particle volume is nearly that of the incident wave and Eq. (13b) ensures that the reflection at the sphere is surface is minimal. These conditions define a weakly scattering sphere. The parameter ρ is called the phase shift parameter.

Figure 2 shows a plot of Eq. (12) as a function of the dimensionless parameter $u = qR$. Recall that q is a function of the scattering angle θ, Eq. (5). Figure 2 illustrates four major regimes/features for the scattering. These are:

1. The forward scattering lobe. When $qR < 1$, The scattering is q-independent, hence θ-independent. In this regime, under the conditions of Eqs. (13), the differential scattering cross section is given by the Rayleigh formula for small spheres of arbitrary refractive index

$$d\sigma/d\Omega = R^6 k^4 F(m) \tag{14}$$

   where

$$F(m) = |(m^2 - 1)/(m^2 + 2)|^2 \tag{15}$$

   Given these functionalities, this $qR < 1$ regime, forward scattering lobe can also be called the "Rayleigh regime".

2. The Guinier regime. When $qR \approx 1$,

$$S(q) = 1 - (qR_g)^2/3 = 1 - (qR)^2/5 \tag{16}$$

   where R_g is the radius of gyration of the scattering object. Equation (16) is derived from Eq. (11) by expanding the exponential term to second order [24, 25]. For a sphere, $R_g^2 = (3/5)R^2$, hence the second equality.

3. The power law regime. When $qR > 1$, Fig. 2 shows an envelope for the scattering

having a power law functionality with an exponent of -4. This is often called the Porod regime [25, 26]. It can be shown that in this RDG, diffraction limit, the Porod exponent is equal to − (d + 1) where d is the spatial dimension of the diffracting object [17]. The Porod envelop itself is described by

$$S(q) = 9(qR)^{-4} , \qquad qR > 1 \qquad\qquad (17)$$

.

4. <u>The ripples</u>. A major feature for the scattering curve is the interference ripples. For the RDG limit these ripples have a spacing of
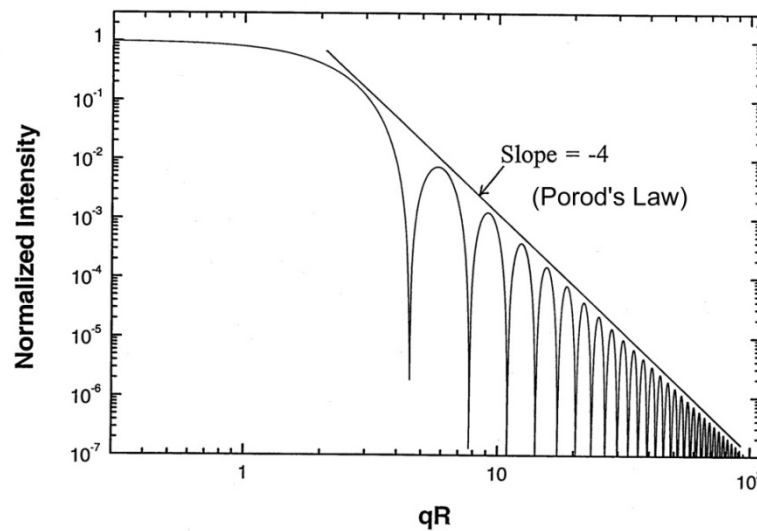
$$\delta(qR) = \pi. \qquad\qquad (18)$$

Figure 2. Plot of the structure factor for scattering from a sphere in the Rayleigh-Debye-Gans limit.

3.2 Mie Scattering.

The Mie solution for describing scattering from a sphere of arbitrary size and refractive index has been existent since 1908 [27], and the advent of modern computers in the 1960's and 70's allowed quick and accurate calculation of the solution (see e.g. [28]). Moreover, the RDG solution for soft spheres has been known since the early 20th century and its description is often juxtaposed closely with the Mie solution in various monographs on the subject of light scattering [18-21]. Thus it is rather curious that historically the Mie solution, to this author's knowledge, is always plotted as scattered intensity versus the scattering angle θ and apparently never plotted, as for the RDG case, using the dimensionless qR, nor not even plotted versus q as diffraction theory would suggest.

In 2000 we [1] began the exploration of plotting Mie scattering in the same manner as shown in Fig. 2, above, viz. I vs. qR log-log, a method we have come to call "Q-space analysis".

When this was done, unforeseen patterns in the scattering were discovered that provide useful new descriptions of the scattering. Perhaps the most startling patterns occur at large qR, and it is there the following description starts.

   3.2.1 The power law regime, qR > 1. Figure 3a shows an example of Mie scattering (I_{VV}, incident and detected polarization vertical) for a sphere with an index of refraction *m* = 1.05 and a variety of sizes expressed as the size parameter kR. The intensity normalized by its value at zero scattering angle I(θ)/I(0) is plotted versus the scattering angle θ. A series of bumps and wiggles are seen with some periodicities, but with no particular coherent pattern. The scattering angle θ, although conveniently measured in the laboratory, uncovers no patterns.
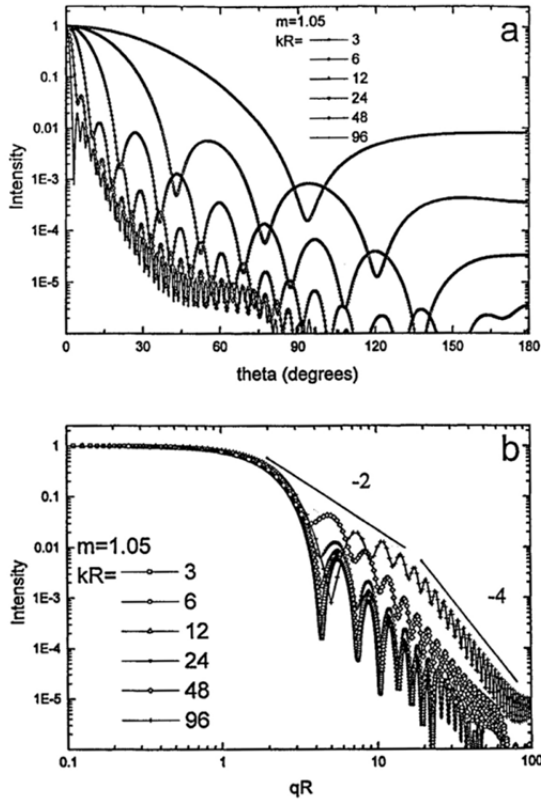

Figure 3. (a) Normalized Mie scattering curves as a function of scattering angle for spheres of refractive index *m* = 1.05 and a variety of size parameters; and (b) same as (a) but plotted logarithmically vs. *qR*. Lines with slope -2 and -4 are shown [1].

   Figure 3b shows the same data but plotted versus the dimensionless qR logarithmically. Now the plots for the different size parameters appear to be related in a coherent manner, and power laws describing the envelopes of the plots at large qR are apparent.

Figure 4 shows the same comparison as seen in Fig. 3 only for an index of refraction of 1.5. Figure 4a shows the conventional plot versus scattering angle and again chaos reigns. Figure 4b shows the same data plotted in q-space and again power laws appear.
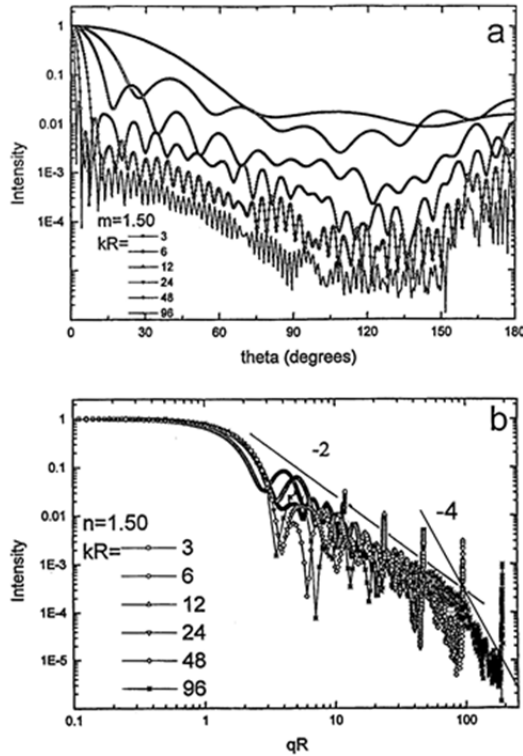

Figure 4. (a) Normalized Mie scattering curves as a function of scattering angle for spheres of refractive index $m = 1.50$ and a variety of size parameters; and (b) same as (a) but plotted logarithmically vs. qR. Lines with slope -2 and -4 are shown [1].

Figures 3b and 4b are examples of Q-space analysis; the double logarithmic plotting of the scattered intensity versus either q or qR. Q-space analysis uncovers quantitative patterns unseen or unemphasized before. At small qR a universal "forward scattering lobe" is seen. Near $qR \approx 1$, a Guinier regime appears. At larger qR power law envelopes for the scattering curves appear with -2 and -4 exponents. There is a crossover between these power laws to imply a length scale relevant to the scattering. Finally, the enhanced backscattering, the "glory," shows no particular pattern (none found so far) but is compressed into spikes in the large qR part for each size parameter kR.

A second useful normalization for the scattered intensity is to normalize by the differential Rayleigh scattering cross section of the particle assuming it is a Rayleigh scatterer [4] (which it typically is not). The differential Rayleigh scattering cross section is given by Eqs. (14) and (15) above.

Figure 5 shows the Rayleigh-normalized Mie scattering intensity i.e., $I_{vv} /R^6 k^4 F(m)$. These plots include a small degree of size polydispersity to wash out the ripple structure and hence leave only the envelopes. This figure demonstrates a quasi-universality of Mie scattering

on the phase-shift parameter Eq. (13a), above. For each phase-shift parameter value shown the values of m and kR vary widely. Despite this variation, the curves for the same ρ lie with each other, hence the curves are universal with ρ. This universality is not perfect, however, with variations of approximately a factor of 3 for the same ρ.

Figure 5 also shows that the ρ-crossover between the -2 and -4 power laws is at qR values near 1.2ρ.
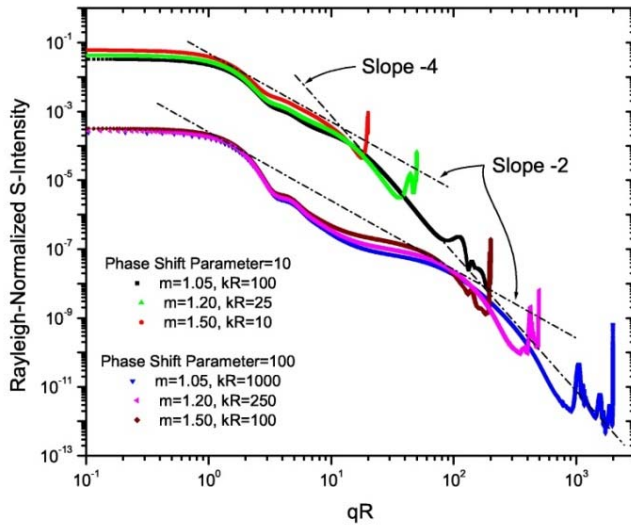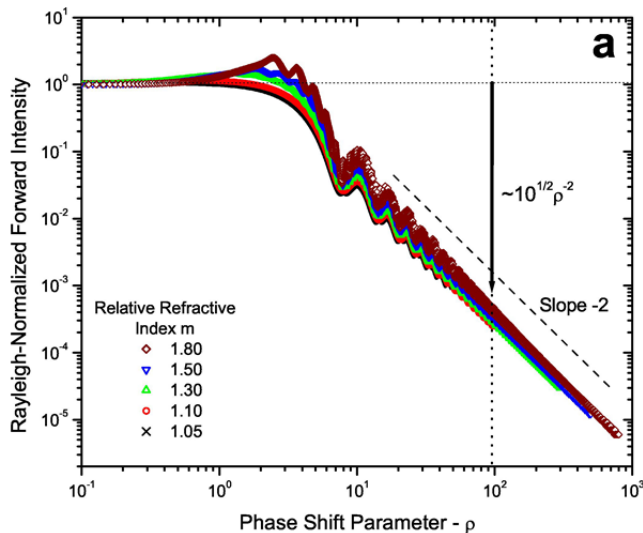

Figure 5. Two sets of Rayleigh-normalized Mie intensity curves for spheres. The three curves in each set have the same value of ρ but different values of kR and m. The bounding envelopes are shown for both sets of curves and illustrate how the envelopes only depend on ρ [4].

3.2.2 The forward scattering lobe, qR < 1. The behavior of the forward scattering lobe (the Rayleigh regime) where qR < 1 is shown as a function of ρ in Fig. 6 for a variety of refractive indices m. For ρ < 1, the Rayleigh formula, Eqs. (14) and (15), accurately describes the forward scattering. On the other hand, for ρ >> 1 the forward lobe scattering is less than that predicted by the Rayleigh formula by a factor of ca. $3/\rho^2$. The crossover between these two regimes is near ρ ≈ 2. While these results are roughly independent of the particle's refractive index a strong ripple structure appears near ρ ≈ 2 to 20 with increasing refractive index.

Figure 6. Rayleigh normalized forward scattering intensity, $I(0)/R^6k^4F(m)$, versus the phase shift parameter ρ [4].

The $3/\rho^2$ factor causes the forward scattering size functionality to fall from R^6 to R^4 and the refractive index functionality to decrease. This combined with the narrowing of the forward lobe, $q \sim$ angle $\sim R^{-1}$ hence solid angle $\sim R^{-2}$, qualitatively explains the crossover of the total

scattering from the Rayleigh R^6 to the geometric R^2 functionality, independent of the refractive index.

   3.2.3 The Guinier regime, qR ≈ 1. Careful inspection of Fig. 4b shows that not all the plots for the different size parameter values lie together in the Guinier regime despite the fact that the plots are made with the dimensionless variable qR. To explore this further we generated Mie scattering curves for known values of the sphere radius hence known radius of gyration through $R_g^2 = (3/5)R^2$ [2]. These where then fit to the Guinier equation, Eq. (16), using the restriction qR ≤ 1. This generated a fit value
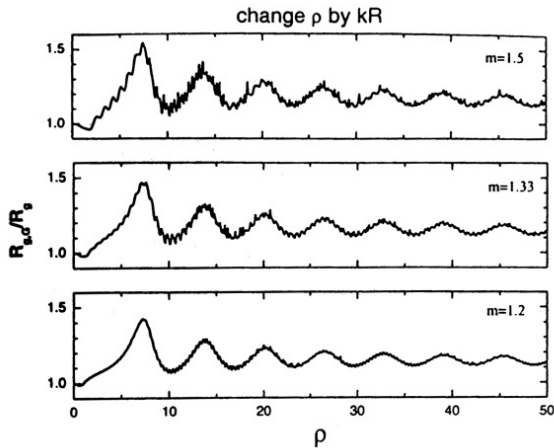
change ρ by kR

m=1.5

m=1.33

m=1.2

Figure 7. The ratio of the Guinier inferred to real radius of gyration $R_{g,G}/R_g$ as a function of the phase shift parameter ρ for spheres with three different refractive indices. The size parameter kR was varied to vary ρ [2].

for the radius of gyration that we called the "Guinier inferred radius of gyration, $R_{g,G}$". This was then compared to the actual R_g.

   Such a comparison is shown in Fig. 7. The ratio $R_{g,G}/R_g$ starts at unity, as it should, for small ρ and then increases and oscillates. The oscillations damp with increasing ρ and in the limit ρ → ∞, $R_{g,G}/R_g$ → 1.12. This value is expected in the geometric limit where the sphere acts like a circular obstacle and Fraunhofer diffraction around the obstacle determines the forward scattering lobe and its Guinier edge. Thus plots such as Fig. 6 describe how the edge of the forward scattering lobe behaves as the scattering evolves from a three dimensional sphere to effectively a two dimensional obstruction. Figure 7 also provides a recipe for spherical particle sizing with at modest knowledge of the refractive index. Finally, the oscillation was shown to be 180° out of phase with similar oscillations in the total scattering efficiency for reasons yet to be determined [2].

   3.2.4 The ripples. The interference ripples in the ρ = 0, RDG limit are equally spaced in qR-space the spacing being δ(qR) = π. As ρ increases the ripple spacing evolves with some small chaos until for ρ ≥ 5, the spacing is uniform in θ-space with the spacing being δθ = π/kR = λ/2R [3]. This latter result, the angle between diffraction or interference minima being the wave length divided by the full dimension of the object, is the classic Fraunhofer result for one dimensional objects, e.g. single and double slits. Ripple spacing can be used for particle sizing [29-31].

   3.2.5 The enhanced backscattering. The enhanced backscattering has so far defied our attempts to find a pattern.

3.3 Summary.

   All these results can be distilled into a new general description of light scattering from a sphere of arbitrary size and real refractive index. There are five major regimes/features for the scattering. These are:

   1. The forward scattering lobe. The description starts with the magnitude of the scattering which uses the forward scattering lobe as its basis. The forward scattering lobe (the Rayleigh regime) lies in the region qR < 1 and is described

by

$$I(0) = R^6 k^4 F(m) \qquad \text{when } \rho < 1 \qquad\qquad (19a)$$

$$I(0) \approx (3/\rho^2) R^6 k^4 F(m) \quad \text{when } \rho > 5 \qquad\qquad (19b)$$

2. <u>The Guinier regime</u>. When $qR \approx 1$,

$$S(q) = 1 - (qR_{g,G})^2/3 \qquad\qquad\qquad (20)$$

where $R_{g,G}$ is related to the actual radius of gyration of the scattering object via curves such as shown in Fig. 7.

3. <u>The power law regime</u>. With the normalization of Eqs. (19), there are three power law regimes (including the rather trivial forward scattering lobe) that are quasi-universal with ρ

$$I \sim (qR)^0 \qquad \text{when } qR < 1 \qquad\qquad (21a)$$

$$I \sim (qR)^{-2} \qquad \text{when } 1 < qR < 1.2\rho \qquad\qquad (21b)$$

$$I \sim (qR)^{-4} \qquad \text{when } qR > 1.2\rho \qquad\qquad (21c)$$

4. <u>The ripples</u>. Ripples appear in the non-trivial power law regimes with $qR > 1$. The ripple spacing is

$$\Delta\theta = \pi \qquad\qquad \text{when } \rho < 5 \qquad\qquad (22a)$$
$$\delta(qR) = \pi/kR \quad \text{when } \rho > 5 \qquad\qquad (22b)$$

5. <u>The Glory</u>. Enhanced backscattering, the Glory, appears when $\rho > 5$. No patterns have yet been discerned to describe the Glory.

This general description is portrayed graphically in Fig. 8 which shows the envelops of the scattering curves, ignoring the ripples and backscattering, plotted versus q (not qR). Two points of view are given: Fig. 8a where the scattering is normalized by the Rayleigh scattering, and Fig. 8b where the scattering is normalized by the forward scattering.

More than a summary, Fig. 8 shows how Mie scattering patterns evolve with increasing ρ. The story of scattering from a dielectric sphere starts at $\rho = 0$ with the Rayleigh-Debye-Gans limit. This is the diffraction limit for which each sub-volume of the scattering object sees only the incident wave. For $qR < 1$ the forward scattering lobe of the RDG curve is flat, i.e., $(qR)^0$, and the magnitude of the scattering is equivalent to the Rayleigh scattering prediction, Eqs. (14) and (15). There is a change in slope near $q \approx R^{-1}$, the Guinier regime, indicating the length scale of the sphere, its radius. For $qR > 1$ the envelop functionality falls off with a negative four power law, the Porod limit, with magnitude $9(qR)^{-4}$ times the Rayleigh scattering cross section. This description includes Rayleigh scattering in the limit $\lambda \gg R$ because then $qR < 1$ and only the flat part of the scattering function is obtained.

When $\rho > 1$, scattering in the forward lobe regime *decreases relative* to the Rayleigh scattering value. The relative decrease (remember, the unnormalized scattering increases with ρ) is proportional to a factor of $\rho^2/3$ as depicted in Fig. 8a. Again near $qR \approx 1$, a Guinier regime

indicates the particle size. For $qR > 1$ the scattering now falls off roughly as $(qR)^{-2}$ until this functionality crosses the RDG curve near $qR \approx 1.2\rho$. For $qR > 1.2\rho$ the scattering is identical to
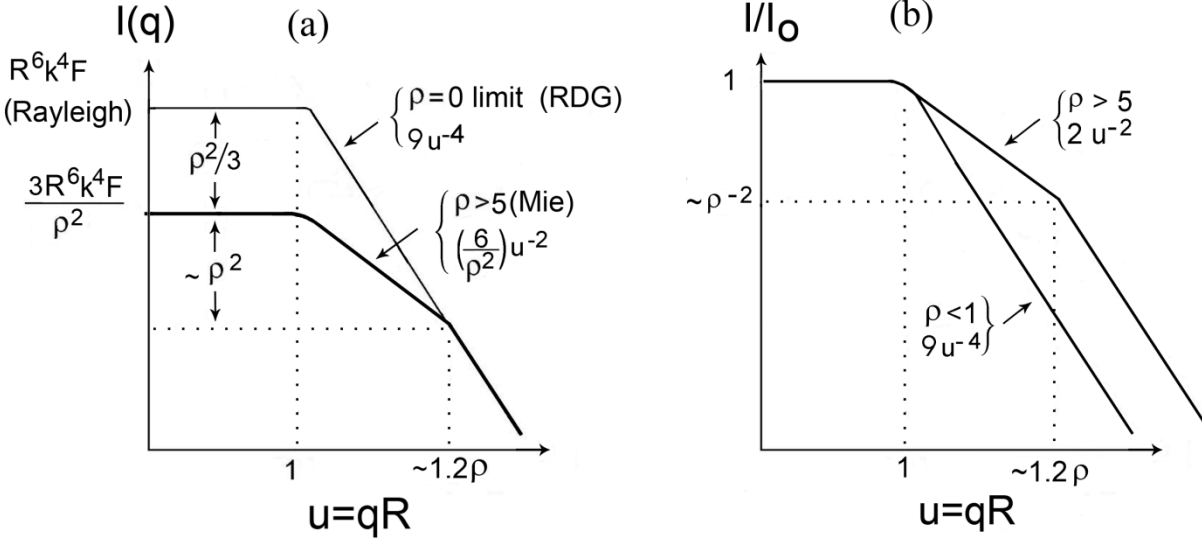

Figure 8. Diagrams of the general description of Mie scattering, the Mie scattering patterns, for uniform spheres of arbitrary size and real refractive index.

RDG scattering, falling off as $9(qR)^{-4}$ times the Rayleigh cross section for all R and m as long as $qR > 1.2\rho$. The $(qR)^{-2}$ functionality between $qR = 1$ and ca. 1.2ρ is exact only at those limits; the average Mie curves dip below the $(qR)^{-2}$ line. This dip is the first interference minimum present in all Mie curves and is the strongest of all the minima. Its position is near qR ~3.5.

4. Explanations of the patterns.

4.1 The shell model. The general features for the envelopes of the scattering depicted in Fig. 8 can be replicated by assuming that when $\rho > 5$, the interior of the sphere is dark and the scattering comes from a shell just inside the outer surface, illuminated by the incident wave [1]. Then the scattering profile is simply the square of the Fourier transform of the shell, which would be RDG scattering from the shell. The result is

$$S(q) = [3(\sin u - u\cos u - \sin v + v\cos v)/(u^3 - v^3)]^2. \qquad (23)$$

In (23) $u = qR_o$ and $v = qR_i$ where R_o and R_i are the inner and outer radii of the shell, respectively. Equation (23) yields a forward scattering lobe limited by a Guinier region near $qR_o \approx 1$, followed by a power law envelope described by ca. $2u^{-2}$, then a crossover to another power law of u^{-4}. These are all in quantitative agreement with the Mie features shown in Fig.8b. The crossover is at $2R_o/(R_o - R_i)$. If this is set equal to ρ, one finds a shell thickness of $R_o - R_i = \lambda/[2\pi(m - 1)]$. Given this shell thickness, one can calculate the volume of the shell in terms of this ρ value. For a thin shell, the Rayleigh differential scattering cross section can be calculated for the forward scattering lobe to be $(12/\rho^2)R_o^6k^4F(m)$. This has the same functionality as the Mie result, Eq. (19b).

The only problem with the shell model is that it is wrong. It is based on the erroneous assumption that the interior field is a shell. Calculations readily show that the interior field is quite complex for large ρ and bears no resemblance to a shell. Thus one is left to wonder why the model works so well and frustrated that it can't be right.

4.2 Phasor analysis. Berg and coworkers [6] have developed a microphysical model based on the Maxwell volume integral representation of the scattering process. The scattered wavelets from sub-volumes of the sphere's interior are represented by phasors. With these one can visualize how the total scattered field, the sum of the phasors, evolves with changing ρ and q. The analysis for ρ < 1 shows that the forward scattering lobe occurs at small q because then all the phasors add together constructively. The Guinier crossover occurs as the phasors begin to fall out of phase as indicated by a spread in their pointing directions. The $(qR)^{-4}$ Porod regime is a consequence of destructive interference of wavelets from the entire body of the sphere except those from the tips or end caps of the sphere along the ±q-direction. Finally, the ρ-crossover is a result of wavelets from the sphere's interior field hot spots destructively interfering. Importantly it was shown that the length scale implied by the ρ-crossover correlates well with the size of the hot spots.

5. Scattering from non-spheres.

The obvious questions to address now are: What does scattering from other particle shapes or configurations show when subjected to Q-space analysis (I vs. q, log-log)? Do power laws appear; with what exponents? Is it true that scattering from other particle shapes and assemblies also starts at the Fourier limit? If so, how do the power laws evolve with increasing ρ? In what follows we will begin to answer these questions by considering a number of different non-spherical particles. Remarkably, when we do, we will again find power laws.

5.1 Spheroids. Recently Berg has studied scattering from dielectric spheroids using the T-Matrix method [21] to calculate scattering curves for a variety of particles [15]. He found power laws very similar to those found for spheres: a forward scattering lobe followed by a Guinier regime, then a $(qa)^{-2}$ regime (a is the major axis), a ρ-crossover to a Porod regime. Differences from spheres appeared, however, with increasing difference of the aspect ratio from unity. An example is shown in Fig. 9 which displays a $(qa)^{-5.5}$ power law beyond the ρ-crossover.
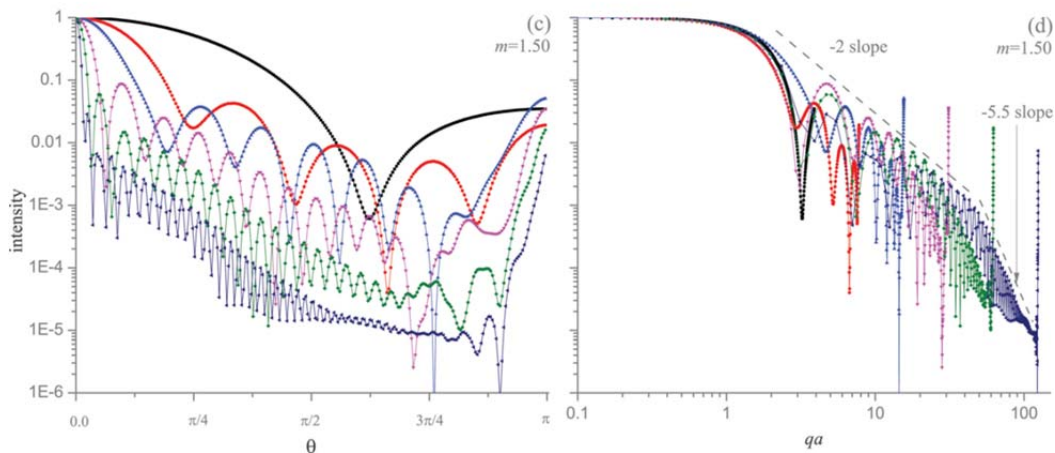

Figure 9. Scattered intensity for strongly refractive prolate spheroids with an aspect ratio of 0.8 and size parameters ka, where a is the major axis of the spheroid, ranging from 1.94 to 62.2. The incident illumination is parallel to the major axis. On the left the normalized intensity is plotted versus the scattering angle, on the right plotted versus the log of qa.

5.2 Fractal aggregates. Figure 10 shows a scattering curve for an ensemble of fractal aggregates formed via diffusion limited cluster aggregation (DLCA), plotted I vs. q log-log. Much like for spheres, and now spheroids, the plot displays a flat Rayleigh regime at small q that curves over near $qR_g \approx 1$ to a power law at large q. For fractal aggregates the power law exponent is the negative of the non-integer aggregate fractal dimension of the aggregate [16, 17, 32]. The data in Fig. 10 are for a polydisperse ensemble of aggregates that very likely have random orientations. They are typical of a large number of fractal aggregate situations.

Visible inspection of a typical colloidal or aerocolloidal DLCA fractal aggregate shows an assembly of roughly spherical primary particles less than 50 nm in diameter stuck together in an open, branched chains. This open, aggregate morphology is very different than the compactness of spheres and spheroids.

The RDG theory successfully explains data such as those in Fig. 10 [16]. That is, the square of the Fourier transform of the aggregate structure, the structure factor, describes the shape of the plot. The differential scattering cross section is the structure factor multiplied by the square of the number of monomers in the aggregate and the Rayleigh scattering cross section for an individual monomer. This is equivalent to Eq. (19a) for spheres. A semi-quantitative argument that the RDG description applies to aggregates with a fractal dimension less than 2 in the limit of large aggregates exists [16].
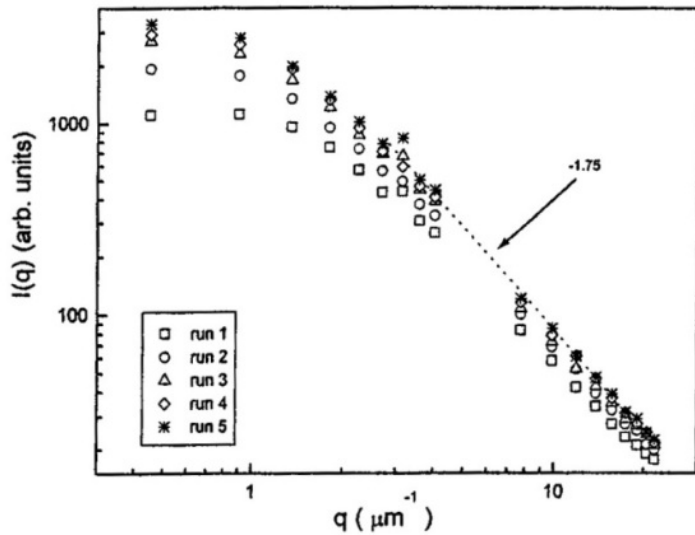

Figure 10. Scattered intensity as a function of the wave vector q for a TiO_2 aerosol. The slope in the large q regime for this log-log plot is the fractal dimension D_f=1.75. Five sets of data represent five consecutive runs as aggregation ensued.

The structure factor of a single aggregate is rarely described by a nice smooth power law plot as shown in Fig. 10, but this is true of the real space power laws too [33]. Hence Fig.10 must be viewed as a statistical average.

5.3 Dusts. Very recently I have applied the Q-space analysis [13] to a well-known data set [34, 35] for scattering from desert dusts. An example is given in Fig. 11. Figure 11a shows the data plotted in the conventional way, log(I) versus θ. A non-descript curve is seen. Figure 11b shows the same data plotted log(I) versus log(q), i.e. Q-space analysis, now a quantifiable power law is uncovered. Similar results were found for volcanic ashes and Martian surrogate particles [13]. Unfortunately, no data were obtained in the Guinier and Rayleigh regimes (qR ≤ 1). Regardless, we find yet more power laws this time associated with a variety of dusts with associated exponents of ca. 1.7 to 1.8 that beg for explanation.
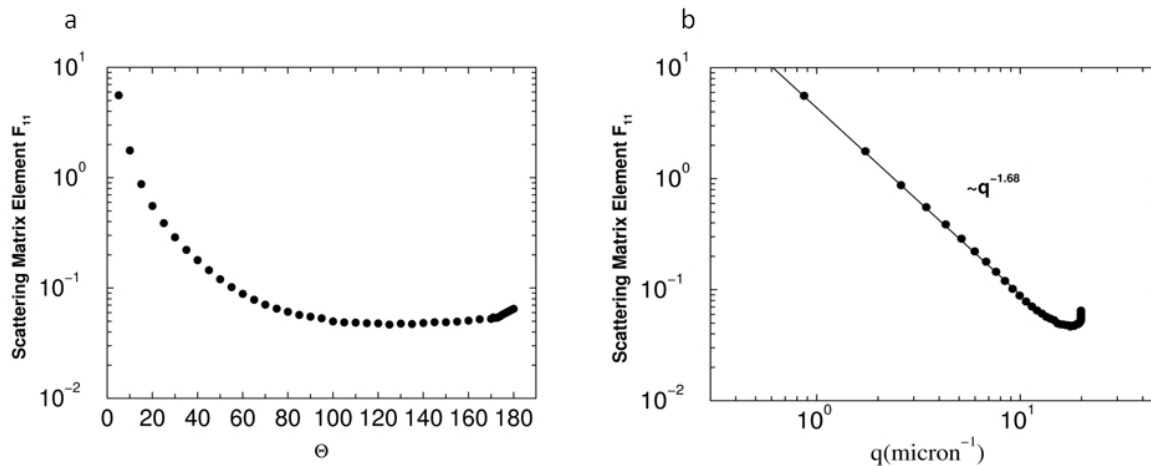
Figure 11. The scattered intensity (scattering matrix element F_{11}) for Saharan (JGR 112 [34]) dusts versus (a) scattering angle θ, and (b) The scattering wave vector q.

In an effort to replicate theoretically the scattering from dusts Zubko has used DDA to calculate the scattering by four types of irregularly shaped particles which he calls pocked spheres, rough surface spheres, strongly damaged spheres and agglomerated debris at three different relevant refractive indices [35]. In collaboration with Zubko we have found once again that Q-space analysis of all nearly all these situations shows power laws [14]. An example is given in Fig. 12.
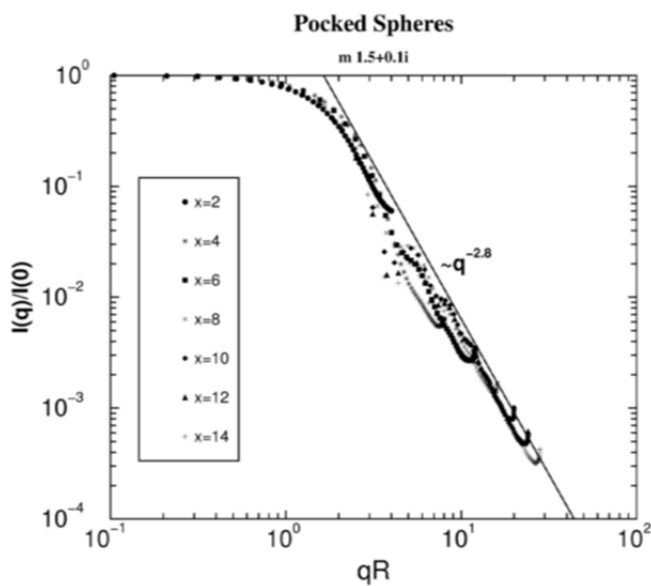

Figure 12. Normalized scattering intensity calculated for pocked spheres of various size parameters, x = kR.

6. Significance of the Q-space analysis and the resulting patterns

The Q-space analysis uncovers a physical description of Mie scattering by dielectric spheres. Mie scattering starts as simple diffraction at the ρ = 0 limit and then systematically evolves with increasing ρ. This diffraction or RDG limit at ρ = 0 is simply the square of the Fourier transform of the particle's physical structure. This limit holds when the interior of the

particle is uniformly illuminated by the incident field. The parameter ρ is a measure of the extent of interaction between the infinitesimal sub-volumes of the particle. With increasing ρ, these sub-volumes experience not only the incident field, but also begin to experience the scattered fields of their neighbors, a condition expressed by the term "internal multiple scattering". The interior multiple scattering darkens the interior by a combination of a decrease of the wave amplitude and randomization of the phases. This darkening causes the forward scattering to decrease relative to the Rayleigh scattering, incident field illuminated situation at $\rho = 0$. The quantitative aspects of this decrease are a crossover from R^6 to R^4 size functionality and a severe decrease in the refractive index functionality (perhaps a complete loss). When q is large enough, so that inverse q is comparable to the size of the interior hot spots, the hot spots dominate the scattering. Remarkably, this causes the total scattering to regain its $\rho = 0$ value in the region qR > 1.2ρ. The combination of the relative decrease in forward scattering intensity ending at qR $\approx$ 1 and the $\rho = 0$ value intensity beginning at qR > 1.2ρ leads to the appearance of a $(qR)^{-2}$ regime in between.

From an empirical point of view, it is very important to stress that the differences and similarities between spheres, spheroids, fractal aggregates and dusts are readily discerned and quantitatively differentiated with Q-space analysis, but unresolvable when plotted conventionally versus theta. With log(q) one gets distinguishable lines and quantifiable exponents, with θ one just gets a bunch of indistinguishable curves (e.g. Fig.11). Q-space analysis could well be a comprehensive and discriminating analysis method of scattering that encompasses all shapes.

For any particle shape the evolution of the scattering with increasing ρ reminds us that the scattering of light is foremost the scattering of waves. Thus scattering is fundamentally diffraction, the mathematical embodiment of which is the Fourier transform, which is both powerful and well understood. At $\rho = 0$, the interior field of any object is simply the uniform incident field hence diffraction from this situation yields the Fourier transform of the object's structure. With increasing ρ, which is a measure of the overall refractivity of the particle, internal multiple scattering changes the internal field, but diffraction from this field still determines the far field scattered wave.

7. Conclusions.

The Q-space analysis of light scattering by particles yields a new perspective from which to describe and understand scattering. It uncovers power law functionalities on the wave vector q for the angular scattering dependence and length scale dependent crossovers between the power laws; it systematically describes the magnitude of the scattering and the interference ripple structure that often underlies the power laws. The analysis has been applied to scattering from dielectric spheres of arbitrary size and refractive index (Mie scattering), fractal aggregates and irregularly shaped particles such as dusts. The simple and comprehensive description of scattering in terms of quantifiable power laws can be used to differentiate scattering by particles of different shapes. The analysis yields a physical understanding of scattering based on diffraction.

REFERENCES

[1] Sorensen CM, Fishbach JD. Patterns in Mie scattering. Opt Commun 2000;173:145–53.

[2] Sorensen CM, Shi D. Guinier analysis for homogeneous dielectric spheres of arbitrary size. Opt Commun 2000; 178: 31–6.

[3] Sorensen CM, Shi D. Patterns in the ripple structure of Mie scattering. J Opt Soc Am A 2002;19(1):122–5.

[4] Berg MJ, Sorensen CM, Chakrabarti A. Patterns in Mie scattering: evolution when normalized by the Rayleigh cross section. Appl Opt 2005; 44(34): 7487–93.

[5] Hubbard JA, Eckels SJ, Sorensen CM. Q-space analysis applied to polydisperse, dense random aggregates. Part Part Syst Charact 2008; 25: 68–73.

[6]] Berg MJ, Sorensen CM, Chakrabarti A. Explanation of the patterns in Mie theory. J Quant Spectrosc Radiat Transfer 2010; 111: 782–94.

[7] Xu M, Alfano RR. More patterns in Mie scattering. Opt Commun 2003; 226: 1–5.

[8] Weinert DW, Cleary TG, Mulholland GW, Beever PF. Light scattering characteristics and size distribution of smoke and nuisance aerosols. In: Evans DD, editor. In: Proceedings of the seventh international symposium on fire safety Science. International Association for Fire Safety Science, Gaithersburg, MD, USA; 2003. p. 209–20.

[9] Jonsson JC, Smith GB, Niklasson GA. Experimental and Monte Carlo analysis of isotropic multiple Mie scattering. Opt Commun 2004;240 :9–17.

[10] Jonsson JC, Karlsson L, Nostell P, Nikasson GA, Smith GB. Angle- dependent light scattering in materials with controlled solar properties. Sol Energy Mater Sol Cells 2004; 84(1–4): 427–39.

[11] Jonsson JC, Smith GB, Deller C, Roos A. Directional and angle- dependent optical scattering of high-performance translucent poly-mer sheets for energy-efficient lighting and skylights. Appl Opt 2005; 44(14): 2745–53.

[12] Shu J, Wilson KR, Ahmed M, Leone S, Graf C, Ruhl E. Elastic light scattering from nanoparticles by monochromatic vacuum-ultraviolet radiation. J Chem Phys 2006; 124 034707-1-9.

[13] Sorensen CM. Q-space analysis of scattering by dusts. J Quant Spectrosc Radiat Transfer 2013; 115:93- 93, http://dx.doi.org/10.1016/j.jqsrt.2012.09.001.

[14] Sorensen CM, Zubko E, Heinson W, Chakrabarti A. Q-Space Analysis of Scattering by Small Irregular Particles. J Quant Spectrosc Radiat Transfer, submitted.

[15] Berg MJ. Power-law patterns in electromagnetic scattering: A selected review and recent progress. J Quant Spectrosc Radiat Transfer (2012), http://dx.doi.org/10.1016/j.jqsrt.2012.05.015.

[16] Sorensen CM. Light scattering by fractal aggregates: a review. Aerosol Sci Technol 2001; 35: 648–87.

[17] Oh C, Sorensen CM. Scaling approach for the structure factor of a generalized system of scatterers. J Nanopart Res 1999; 1: 369–77.

[18] van de Hulst HC. Light scattering by small particles. New York: Dover; 1981.

[19] Kerker M. The scattering of light and other electromagnetic radiation. New York: Academic Press; 1969.

[20] Bohren CF, Huffman DR. Absorption and scattering of light by small particles. New York: John Wiley & Sons; 1983.

[21] Mishchenko MI, Travis LD, Lacis AA. Scattering, absorption, and emission of light by small particles. Cambridge: Cambridge University Press; 2002.

[22] Born M, Wolf E. Principles of Optics. 7th ed. Cambridge: Cambridge University Press; 1999. p.104.

[23] Berg MJ, Videen G. Digital holographic imaging of aerosol particles in flight. J Quant Spectrosc Radiat Transfer 2011; 112: 1776- 1783.

[24] Guinier A. La diffraction des rayons X aux tres petits angles: application a l'etude de phenomenes ultramicroscopique 1939 Ann. Phys.; 12:161– 237.

[25] Guinier A, Fournet G, Walker CB, Yudowitch KL. Small-angle scattering of X-rays. New York: John Wiley; 1955.

[26] Porod G. Die rontgenkleinwinkelstreuung von dichtgepackten kolloiden Systemen.1., Kolloid Z. 1951; 124:83–114.

[27] Mie G. Beitrage zur optik truber medien speziell kolloidaler metallosungen. Ann. Phys. 1908; 25: 377–445.

[28] Denman HH, Heller W and Pangonis WJ. Angular scattering functions for spheres. Detroit: Wayne State University Press; 1966.

[29] Maron SH, Elder ME. Determination of latex particle size by light scattering I. Minimum intensity method. J. Colloid Sci. 1963; 18: 107–118.

[30] Pierce PE, Maron SH. Prediction of minima and maxima in intensities of scattered light and of higher order Tyndall spectra. J. Colloid Sci. 1964; 19: 658–672.

[31] Kerker M, Farone WA, Smith LB, Matijevic E. Determination of particle size by the minima and maxima in the angular dependence of the scattered light. Range of validity of the method. J. Colloid Sci. 1964; 19: 193–200.

[32] Martin JE, Hurd AJ. Scattering from fractals, J. Appl. Cryst. 1987; 20: 61- 78.

[33] Zhang HX, Sorensen CM, Ramer ER, Olivier BJ, Merklin JF. In Situ Optical Structure Factor Measurements of an Aggregating Soot Aerosol, Langmuir 1988; 4: 867-871.

[34] Volten H, Munoz O, Rol E, de Haan JF, Vassen W, Hovenier JW, Muinonen K, Nousiainen T, Scattering matrices of mineral aerosol particles at 441.6 nm and 632.8 nm. J Geophys Res 2001; 106: 17375-17401.

[35] Munoz O, Volten H, Hovenier JW, Nousiainen T, Muinonen K, Guirado D, Moreno F, Waters LBFM, Scattering matrix of large Saharan dust particles: Experiments and computations. J Geophys Res 2007; 112:D13215.

[36] Zubko E, Shkuratov Y, Kiselev NN, Videen G. DDA simulations of light scattering by small irregular particles with various structure, JQSRT 2006; 101: 416- 434.